Proceedings of the ASME 2015 International Design Engineering Technical Conferences & Computers and Information in Engineering Conference
IDETC/CIE 2015
August 2-5, 2015, Boston, MA, United States of America

DETC2015-47313

PATH PLANNING AND CONTROL FOR AUTONOMOUS NAVIGATION OF SINGLE AND MULTIPLE MAGNETIC MOBILE MICROROBOTS

Sagar Chowdhury, Wuming Jing, Peter Jaron, and David J. Cappelleri
School of Mechanical Engineering
Purdue University, West Lafayette
West Lafayette, Indiana 47907
{sagar353, jing6, pjaron, dcappell}@purdue.edu

ABSTRACT

In this paper, we have developed an approach for autonomous navigation of single and multiple microrobots under the influence of magnetic fields generated by electromagnetic coils. Our approach consists of three steps. First, we have developed a heuristics based planning algorithm for generating collision-free trajectories for the microrobots that are suitable to be executed by the available magnetic field. Second, we have modeled the dynamics of the microrobots to develop a controller for determining the forces that need to be generated for the navigation of the robots along the trajectories at a suitable control frequency. Finally, an optimization routine is developed to determine the input currents to the electromagnetic coils that can generate the required forces for the navigation of the robots at the controller frequency. We have validated our approach by simulating two electromagnetic coil systems. The first system has four electromagnetic coils designed for actuating a single microrobot. The second system has an array of sixty-four magnetic microcoils designed for generating local magnetic fields suitable for simultaneous independent actuation of multiple microrobots.

1 INTRODUCTION

Manipulation of micro and nanoscale objects is considered as the enabling step for many biological and manufacturing tasks that might potentially revolutionize the respective industry. For example, manipulation of cells to form a pattern can enable cell based assembly, study of cell behavior in a group, diagnosis for therapy, etc. On the other hand, the ability to assemble heterogenous microscale components into an intricate functional device can potentially benefit energy, communication, and computing industry. Microfluidics [1], electrostatic [2], magnetic manipulation [3,4], Atomic Force Microscopy (AFM) [5],optical tweezers (OT) [6, 7, 8], and micro-grippers [9] are some of the enabling technologies proposed for micro and nanoscale manipulation.

Das *et al.* [9] developed a 3D deterministic microassembly setup known as μ^3. The platform consists of three manipulators with resolution of 3 *nm*. The manipulators can provide both serial and parallel assembly operations under SEM. The base manipulator has custom designed fixtures and a custom designed hotplate for processing abilities. The system is equipped with 3D stereo vision for part detection, calibration, trajectory planning, and assembly sequence execution. The authors have used the platform for MEMs assembly operations based on snap fasteners. The overall workspace is reported as 8 cm^3. Cappelleri *et al.* [10, 11] also developed a flexible micro-assembly setup with multiple fixed manipulators for automated manipulation and assembly of micro-scale parts.

Hoover and Fearing [12] have been working on developing a microgripper system that can provide high functionality for micro assembly operations. Their focus is in designing highly flexible microgrippers by using smart compliant mechanisms to increase the effectiveness of gripper based microassembly operations.

Probst *et al.* [13] have been working on integrating optomechatronic devices with vision feedback to improve the res-

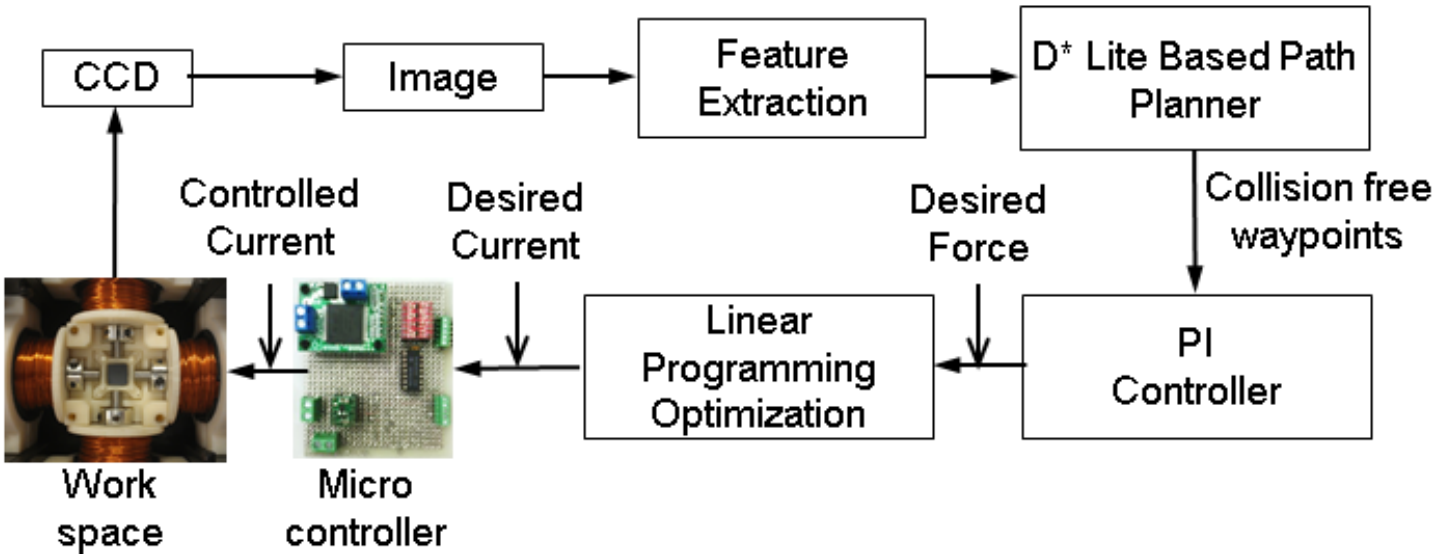

Figure 1: The overall approach: The approach consists of tight integration of perception, planning, control, and optimization.

olution of manipulator based microassembly. Fatikow *et al.* [14] have developed a microassembly station with two microrobots installed in two piezo-electrically driven bases. Each of the robots has a 5 DOF manipulator that is able to perform assembly operations.

Bohringer *et al.* [15] have been working on developing technology for parallel assembly. They have developed a new approach for microassembly by using ultrasonic vibration to prevent sticking of the parts and then applying electrostatic forces to position the parts with perfect alignment.

Diller *et al.* [16] developed several reconfigurable magnetic micromodules (Mag-Mods) for assembly and disassembly operations. They achieved independent locomotion of these modules by using electrostatic surfaces. By selectively activating a particular surface the attached robot-module can be immobilized while the other modules can be moved using the gross magnetic field generated by six coils. Each module is a permanent magnet which limits its application only to the assembly of the objects that are magnetic in nature. In another work [17], they demonstrated the pushing based manipulation with Mag-Mods. However, the magnetic field generated by six coils cannot be controlled locally. Instead, multiple heterogeneous Mag-Mods are manufactured that respond differently to the same magnetic field. By utilizing their dynamical behavior in response to the same magnetic field, the robots can be controlled independently.

Pelrine *et al.* [18] developed a swarm of robots arranged on a printed circuit board (PCB). Each robot is a *mm* scale magnet and is actuated by magnetic field generated by a PCB. The PCB generates localized magnetic fields for individual control of the robots. Using the swarm of robots, massive parallelization in assembly operation can be achieved. The system is capable of fast manipulation. The demonstration showed 73 robots performing coordinated moves each at 19 moves/sec. The total system rate is 1386 ($\sim 73 \times 19$) moves/sec.

Optical tweezers (OT) have been utilized both for microscale assembly [19, 20] and biological manipulation [21, 22]. Highly focused laser beams are used to move and orient parts in 3D with high precision. By coordinating multiple laser beams highly precise assembly tasks can be realized. However, OT based assembly operation suffers from slow speed. Moreover, the small workspace ($100\,\mu m \times 100\,\mu m$) makes it more suitable for biological manipulation than manufacturing applications. Hu *et al.* [23] utilized the heating energy of laser to control the movements of bubbles for manipulation and assembly of microscale objects.

Traditional microscale assembly technologies are dominated by robotic pick-and-place machines and machine vision where accuracy and speed of operation need to be compromised. Sariola *et al.* [24] are aiming to utilize microscale physics (i.e. surface tension) for self-alignment along with the use of traditional robotic tools to improve the accuracy and speed of microassembly.

The microassembly techniques mentioned above can be divided into two groups: fixed manipulator [9, 10, 11] and mobile manipulator [17, 18]. Fixed manipulators are good for customized assembly operations with high precision. However, the number of manipulators is limited by the physical sizes of the manipulators. More manipulators in the workspace might result in occlusion that can make the automated assembly operation and parallelization difficult. Mobile manipulators actuated by a global magnetic field are also not suitable for parallelized

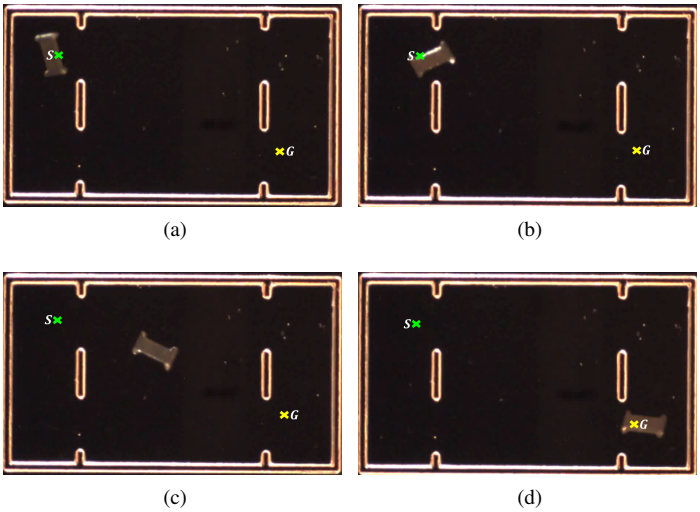

(a) (b) (c) (d)

Figure 2: Transport of a single robot from an initial location to a final location with the actuation of global magnetic filed generated by the system in Figure 4. (a) Initial scene with the robot at a location at "S", (b) The robot align itself towards the next waypoint, (c) The robot moves toward the goal location, and (d) The robot reaches the goal location at "G".

assembly operations since truly independent control of robot is extremely challenging to achieve.

Magnetic manipulation [25, 26, 27] is regarded as a promising technology due to its ability to generate a force ranging from pN to μN, cheap installation, and precision in operation. However, most of the magnetic manipulation setups are designed to create a global magnetic field that can severely affect the flexibility of operation [28, 29, 30]. The ability to automatically control multiple magnets independently can enable high throughput operation.

In this paper, we have developed an approach for automatic navigation of single and multiple magnetic robots in an environment with moving obstacles. Our approach consists of three steps (Fig. 1): (1) computing collision-free trajectories for the robots, (2) Determining the required forces to move the robots with the help of controllers, and (3) optimizing the input currents to the coils to generate the required forces. We have also proposed a new design of an array of microcoils that can actuate multiple robots independently to demonstrate our approach.

2 Motivation

To investigate the difficulty in precisely navigating a robot with a global magnetic field we have fabricated an arena with obstacles as shown in Figure 2. We have manually switched on or off the magnetic field to move the robot from an initial location

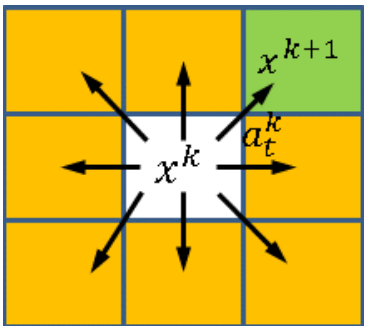

Figure 3: State-action space representation: The action set A consists of eight linear action $a_{t,i}^k$.

to a goal location. The robot starts at the initial location at "S" (Fig. 2a). Due to the obstacle field in the scene the robot needs to circumvent them to reach the goal location. During locomotion, we try to align the robot towards the direction of motion. Hence, in Figure 2b, the robot is rotated by manually switching on multiple coils. Although we can move a single robot in an obstacle field to its goal location at "G" (Fig. 2d), the efficiency of the system as well as the speed of manipulation had to be greatly compromised. Manual control of the exact position of the robot during the course of navigation is challenging; since it is difficult to manually actuate the magnetic field at the required frequency and hence, the robot tends to drift from the desired motion path very easily. Moreover, manual navigation of multiple robots under the influence of local magnetic fields is nearly impossible. Therefore, we have developed an approach for path planning and autonomous navigation of single and multiple robots which is discussed in the following sections.

3 PATH PLANNING

3.1 Problem Formulation

Given:

- Initial states $\{\mathbf{x_{i,init}} = [x_i, y_i]^T\}_{i=1}^n$ of n robots to be transported in X, where X is the discretized operating space of the entire magnetic operating field,
- Goal states of n robots $\{\mathbf{x_{j,goal}}\}_{j=1}^n$ represented as grid locations within X,
- Static and dynamic obstacles $\{\Omega_k\}_{k=1}^l$ represented either as other objects or other moving robots,

Find:

- Collision-free paths $\{\tau_i\}_{i=1}^n$ for n robots to move their goal states $\{\mathbf{x_{j,goal}}\}_{j=1}^m$.

3.2 Approach

Path planning approaches for robot can be divided into two broad classes [31]: (1) Planning with perfect sensor informa-

tion, and (2) planning in uncertain environment. One popular approach is to discretize the workspace into configuration space with the application of graph search [32]. However, this approach gets computationally expensive for high DOF robots. Sampling based search algorithms (RRT, PRM) introduced by Lavalle *et al.* [33] greatly reduced the computational burden.

We use a heuristic graph search algorithm D* Lite [34] for our path planner that can efficiently compute a collision free path for the i^{th} robot from initial state $\mathbf{x_{i,init}}$ to the respective goal state $\mathbf{x_{i,goal}}$. The algorithm is very fast for 2D workspace that we are dealing with in this paper and functions like a backward version of the A* algorithm [32] where the states are incrementally expanded from $\mathbf{x_{i,goal}}$ to $\mathbf{x_{i,init}}$. The other robots and the objects in the scene are regarded as obstacles for the search. We have developed a heuristic to guide the search that can compute the collision free path with expansion of minimum number of states. Rather than starting the search from scratch every time the environment changes, the planner maintains an open set O which contains the states that are more likely to be expanded in the following steps, ranked by their costs. The planner utilizes the open set for replanning and focuses on the states that have a change in costs throughout the entire planning horizon. The planner inserts the states with change in costs due to the change in operating space X into O and continues expanding the states based on the lowest costs until a new path is determined. This provides efficient replanning for multiple robots navigating in a dynamic environment.

3.3 State-action space presentation

The state space of the magnetic workspace is represented as a 2D rectangular grid since we move robots only in the $x-y$ plane. The discrete state $\mathbf{x^k} = \left[x^k, y^k\right]$ of a robot is thus defined as a vector of its position at the time step k that corresponds to a particular grid cell.

An action set $A = \{\mathbf{a^k_{t,1}}, \mathbf{a^k_{t,2}}, \ldots, \mathbf{a^k_{t,8}}\}$ consists of eight *linear* translation actions $\mathbf{a^k_{t,i}}$ available for execution at a given time step k (Fig. 3). All *linear* actions can be represented as follows.

$$\mathbf{a^k_t}\left(\delta x^k, \delta y^k\right) = \begin{bmatrix}\delta x^k \\ \delta y^k\end{bmatrix} \tag{1}$$

where δx and δy are the linear translations along X and Y axis, respectively.

When the magnetic field executes an action $\mathbf{a^k_t}$ at time step k, it transitions from $\mathbf{x^k}$ to $\mathbf{x^{k+1}}$ (Fig. 3) using the following equation.

$$\mathbf{x}^{k+1} = \mathbf{x}^k + \mathbf{a}^k_t \tag{2}$$

3.4 Cost Function

The states from the priority queue O are expanded incrementally with their key values [34] computed as follows

$$\begin{aligned} kv(\mathbf{x}) &= [kv_1(\mathbf{x}), kv_2(\mathbf{x})], \\ &= [min(g(\mathbf{x}), rhs(\mathbf{x})) + h(\mathbf{x_{init}}, \mathbf{x}), \\ &\quad min(g(\mathbf{x}), rhs(\mathbf{x}))] \end{aligned} \tag{3}$$

where $g(\mathbf{x})$ is the optimal cost-to-go from $\mathbf{x}$ to $\mathbf{x_{goal}}$, $h(\mathbf{x_{init}}, \mathbf{x})$ is the heuristic cost estimate of the path between $\mathbf{x}$ and $\mathbf{x_{init}}$, and $rhs(\mathbf{x})$ is the one step look-ahead cost which is calculated as follows

$$rhs(\mathbf{x}) = \begin{cases} 0 & \text{if } \mathbf{x} = \mathbf{x_{goal}}, \\ min_{\mathbf{x'} \in succ(\mathbf{x})}(t(\mathbf{x}, \mathbf{x'}) & \\ +g(\mathbf{x'})) & \text{otherwise} \end{cases} \tag{4}$$

where $succ(\mathbf{x})$ denotes a set of possible resulting states $\mathbf{x'}$ after taking an action $\mathbf{a}$ at state $\mathbf{x}$ and $t(\mathbf{x}, \mathbf{x'})$ denotes the transition cost between $\mathbf{x}$ and $\mathbf{x'}$. In order to ensure optimality, the heuristic function should not overestimate the true cost to $\mathbf{x_{init}}$. The heuristic $h(\mathbf{x_{init}}, \mathbf{x})$ computes the traveled distance for the robot to move between $\mathbf{x}$ and $\mathbf{x_{init}}$. We have used the Eucledian distance between $\mathbf{x}$ and $\mathbf{x_{init}}$ as a measure of $h(\mathbf{x_{init}}, \mathbf{x})$.

We have also utilized the Euclidean distance between $\mathbf{x}$ and $\mathbf{x'}$ to calculate the transition cost $t(\mathbf{x}, \mathbf{x'})$ since we are interested in computing the collision-free shortest path. Hence, $t(\mathbf{x}, \mathbf{x'})$ is formulated as follows

$$t(\mathbf{x}, \mathbf{x'}) = d(\mathbf{x}, \mathbf{x'}) \tag{5}$$

where $d(\mathbf{x}, \mathbf{x'})$ is the Euclidean distance between $\mathbf{x}$ and $\mathbf{x'}$.

4 CONTROLLER DESIGN

4.1 Problem Formulation

In this section, we describe a controller to control the applied magnetic force that is required for the robot to track a waypoint w_p computed in Section 3. The torque to control the orientation of the robot can be derived similarly and is a focus of our future work. The control problem can be derived as follows:

Given:

- The dynamics $m\ddot{\mathbf{x}} + \gamma\dot{\mathbf{x}} + \mathbf{F}_{fric} = \mathbf{F}_{mag}$ of the i^{th} robot, where m is the mass of the robot, γ is the drag force of the surrounding medium, $\mathbf{F}_{mag}$ is the driving magnetic force, $\mathbf{F}_{fric}$ is the surface frictional force, and $i = 1, 2, 3, \cdots n$,
- A reference state $\mathbf{x}_r \in \{\tau_i\}_{i=1}^n$ the robot needs to follow,
- A measurement $\mathbf{x}_m$ of the robot state,

Find:

- A feedback control input $\mathbf{F}_f$ to determine the required magnetic force such that the robot can follow the reference state $\mathbf{x}_r$.

4.2 Approach

The components of the resultant magnetic force $\mathbf{F}_{mag}$ on the robot from the set of the coils can be written as F_x, F_y, and F_z. It is assumed that the robot will be operating in a liquid environment. The γ parameter in the formulation compensates for this. The dynamic behavior of the robot is influenced by several external forces, e.g. Van der Waals, electrostatic, frictional forces etc. Van der Waals and electrostatic forces can be determined with proper experimental procedure. However, we only consider frictional forces for the modeling in this paper since that can be determined from the surface material properties. The frictional force which acts against the direction of motion changes from rest to motion. The robot needs to overcome static friction when starting from rest. On the other hand, dynamic friction comes into play when the robot is in motion. Both the frictional forces can be expressed as follows:

$$\mathbf{F}_{fric} = \begin{cases} \mu_s(W - F_z) & \text{static friction,} \\ \mu_k(W - F_z) & \text{dynamic friction} \end{cases} \tag{6}$$

Where W is the weight of the robot, μ_s and μ_k are the static and dynamic friction coefficients respectively, which depend on the contact surfaces between robot and the workspace. To track a reference state $\mathbf{x}_r$, we apply a PI controller (proportional plus integral) to derive the required magnetic force as follows:

$$\mathbf{F}_f = k_p(\mathbf{x}_r - \mathbf{x}_m) + k_i \int_0^{t_c} (\mathbf{x}_r - \mathbf{x}_m) dt_c \tag{7}$$

Where $\mathbf{x}_m$ is the measured current position of the robot, t_c is the control frequency, k_p is the proportional gain and k_i is the integral gain respectively.

5 COMPUTATION OF CURRENTS

5.1 Overview

The robots used for navigation are magnetized objects. In this paper, we only focused on controlling the position of the robot. Hence, we just have to control the magnetic force $\mathbf{F}_{mag}$. However, the orientation can be controlled by regulating the magnetic torque in a similar fashion. When placed in a magnetic field the robots experience a magnetic force which is the driving force for moving a robot in a specified trajectory. The magnetic force is proportional to the magnetic field and tries to move the robot to the local maxima. The interaction between the robot and the magnetic field can be described as follows:

$$\mathbf{F}_{mag} = V_r(\mathbf{M} \cdot \nabla)\mathbf{B}(x, y, z) \tag{8}$$

Where, V_r is the volume of the robot, $\mathbf{M}$ is the magnetization of the robot, $\mathbf{B}$ is the magnetic potential produced by the coils, and $\mathbf{F}_{mag}$ is the force experienced by the robot.

The planar microcoils are considered as concentric circles with varying radii for the simulations. Using cylindrical coordinates, the components of magnetic potential at a location of the robot $P(r, 0, z)$ [35] along the z and r axes due to a coil with n_c number of turns and current I_c flowing through it can be expressed as:

$$B_z = \frac{\mu_0 n_c I_c}{2\pi\sqrt{z^2 + (R+r)^2}} \left[\frac{R^2 - z^2 - r^2}{z^2 + (r-R)^2} E_2(k) + E_1(k) \right] \tag{9}$$

$$B_r = \frac{\mu_0 n_c I_c z}{2\pi\sqrt{z^2 + (R+r)^2}} \left[\frac{R^2 + z^2 + r^2}{z^2 + (r-R)^2} E_2(k) - E_1(k) \right] \tag{10}$$

Where, R is the effective radius of the coil, n_c is the number of turns in the coil, μ_0 is the permeability of the free space, $E_1(k)$ and $E_2(k)$ are the elliptical integrals of the first and second kinds, respectively, with $k^2 = \frac{4rR}{z^2 + (R+r)^2}$. The magnetic potentials B_x and B_y along the x and y axes can be computed by taking components of B_r.

The goal of this section is to develop an approach to compute the required currents $\mathbf{I} = \{I_l\}_{l=1}^m$ in m coils in the vicinity of the robot that can drive the robot along the specified direction. The equations 8,9, and 10 suggest that there is a non-unique solution to this. Thus, we have formulated an optimization problem to determine the best solution.

5.2 Optimization Problem Formulation

The goal is to minimize the total amount of current in the coils that can generate the required force $\mathbf{F}_f$ computed by the feedback controller in section 4.1. The overall optimization problem can be summarized as follows:

$$\begin{aligned} \underset{\mathbf{I}}{\text{minimize}} \quad & f_0(\mathbf{I}) = \sum_{l=1}^{m} I_l \\ \text{subject to} \quad & -\mathbf{F}_{mag} \leq \mathbf{F}_f \\ & I_{min} \leq I_l \leq I_{max},\ l = 1, \ldots, m. \end{aligned} \tag{11}$$

5.3 Approach

We have cast the optimization problem in equation 11 as a linear programming problem. The constraint is applied as an inequality constraint since equation 8 is a function of $\mathbf{I}$. We have

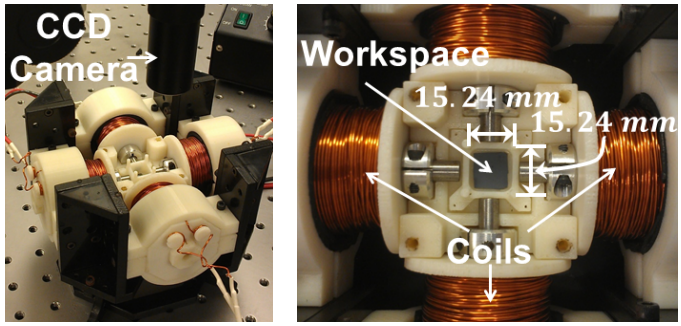

(a) (b)

Figure 4: 4-coil system to actuate a single robot: (a) Full view of the compact system with four coils distributed in the same plane equipped with an overhead CCD camera; (b) Close-up view of the workspace.

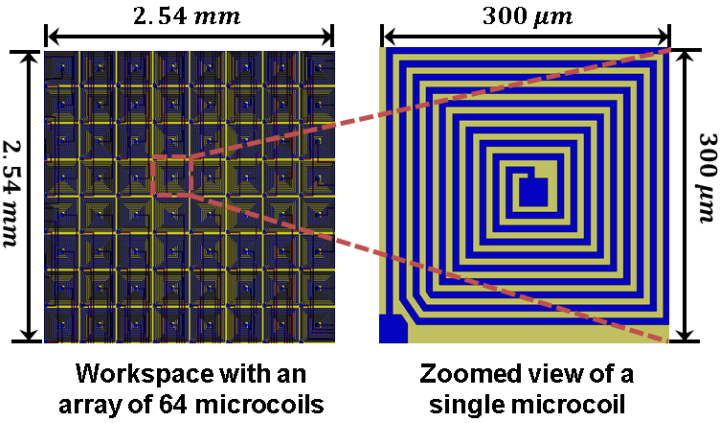

Figure 5: Schematic of a 64-coil system for independent actuation of multiple microrobots : The overall workspace with an array of 64 microcoils and a close-up view of a single microcoil.

used the Matlab optimization toolbox to solve for optimized currents in real time.

6 SYSTEM ARCHITECTURE

We have used two different magnetic coil systems to simulate our approach. The first magnetic coil (Fig. 4) system is composed of four magnetic coils each pair orthogonal to each other. The workspace is located at the intersection of the four magnetic fields. The resultant magnetic field due to the four coils is capable of navigating a magnetic robot in the desired direction. The workspace dimension is 15.24 $mm \times 15.24$ mm. The images of the workspace are acquired in realtime with an overhead CCD camera (Point Grey FL2-14S3C, ptgrey.com) equipped with a microscope lens (Edmund VZM 300i, www.edmundoptics.com)

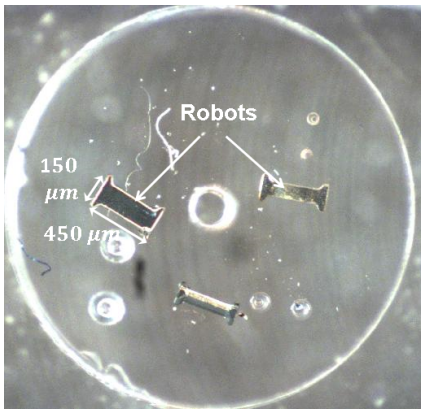

Figure 6: Magnetic microrobots: fabricated using photolithography and metal sputtering.

of adjustable magnification. The combination is able to provide a 8.0 $mm \times 2.0$ mm field of view. The current in each coil can be independently regulated with a customized control unit. Since the magnetic field is global in nature across the workspace it cannot move multiple magnetic robot in independent arbitrary directions at the same time.

To overcome the constraint in independent actuation of multiple robots due to a global magnetic field signal, we have proposed a design of an array of microfabricated planar coils in [35]. Each planar microcoil has a winding width of 7 μm, an out-of-plane winding thickness of 7 μm, and a winding spacing of 7 μm with 10 turns. Each winding is rectangular in shape for the ease of fabrication. For simulation, we have approximated them with concentric circular coils with equivalent radii. That enabled us to utilize existing mathematical expressions in literature to compute the resultant magnetic fields. Each coil is capable of generating a local magnetic field that is dominant only in the vicinity of its location. Figure 5 shows schematic for the design of the microcoil system. The microcoils are designed to be fabricated in three layers to make sure the individual coil leads remain insulated from the other coils. The current in each coil can be controlled through a custom control unit. Each coil is designed to carry a maximum current of 1 amp. However, only the coils in the vicinity of the robot remain in action at a certain point of time. All the 64 coils will not operate simultaneously which would require a maximum current supply of 64 amps.

The robots (Fig. 6) typically used in 4-coil system are manufactured by patterning SU8 photoresist to give the required geometry with dimensions of 450 $\mu m \times 150$ $\mu m \times 50$ μm. On top of the photoresist, nickel (Ni) is sputtered using a physical vapor deposition (PVD) instrument. The thickness of the Ni is set to 500 nm with overall thickness of the robot as 50.5 μm. For the 64-coil system, we have considered the robot made of Neodymium with dimension 300 $\mu m \times 300$ $\mu m \times 250$ μm.

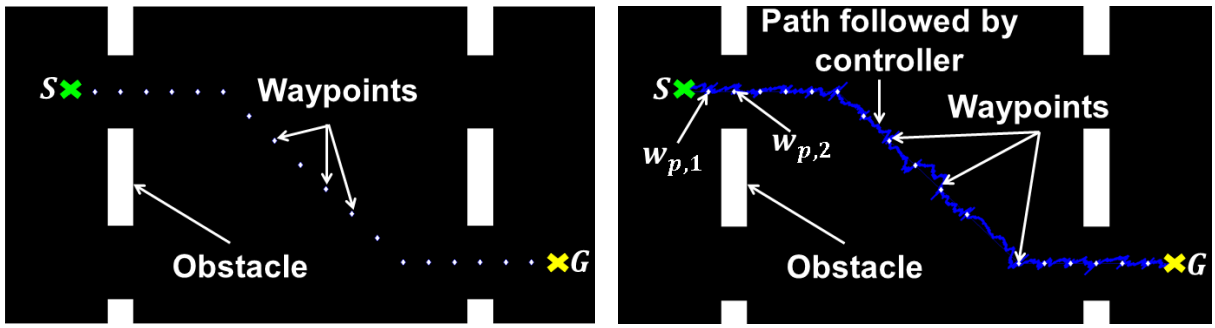

(a) (b)

Figure 7: Autonomous navigation of a single robot in a global magnetic field: (a) Collision free waypoints computed by planner; (b) Path followed by the controller with the presence of measurement noise.

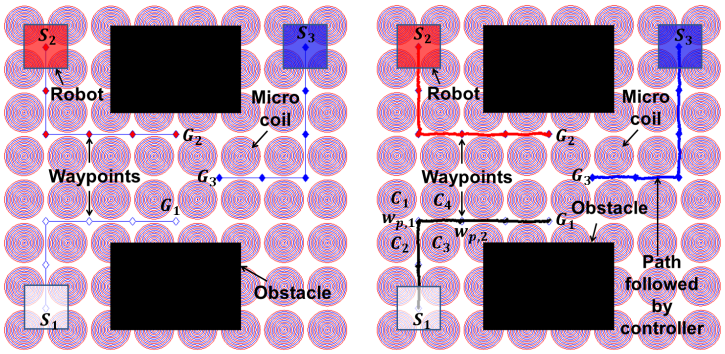

(a) (b)

Figure 8: Autonomous navigation of three robots under the influence of local magnetic fields generated with the array of 64 microcoils: (a) Collision free waypoints computed by planner (the action set consists of four linear actions (top, bottom, right, and left)); (b) Paths followed by the controller with the presence of measurement noise.

Table 1: Simulation Parameters

Parameters	4-Coil System	64-Coil System
Static Friction Coefficient, μ_s	0.3	0.3
Dynamic Friction Coefficient, μ_k	0.15	0.15
No of turns, n_c	250	10
Permeability of air, μ_0 (N/m^2)	1.26×10^{-6}	1.26×10^{-6}
Current limit (A), I_{min} - I_{max}	$0-5$	$0-1$
Robot dimension (μm),	$450 \times 150 \times 50.5$	$300 \times 300 \times 250$

7 RESULTS

We have conducted extensive simulation experiments to demonstrate the effectiveness of our approach. Three representative simulations are described in this section. The planning frequency is set at 50 Hz whereas the controller and optimization loop are run at a frequency of 100 Hz. Since every instance of the planning algorithm is launched separately for the respective robot, the planning and control frequencies are scalable to the higher number of robots as long as there is sufficient computational power available. Moreover, the power of parallelization can be utilized since every instance of the planning algorithm is independent of each other. The noise is modeled by drawing number from a Guassian Distribution with mean 0 and standard deviation 20 μm. The planner gives the next waypoint and the controller computes the required force to track the waypoint. Finally, the optimization loop computes the currents in the coils to generate the force. The parameters used for the simulations are shown in Table 1. The parameters are determined by experimental characterization of the system [29]. The drag coefficient is calculated using the following equation [36]

$$\gamma = \frac{1.328}{\sqrt{Re}} \tag{12}$$

Where, Re is the Reynold's number which can be computed as $Re = \frac{v_r L}{\nu}$. v_r is the velocity of the robot at a particular time instant, ν is the kinematic viscosity of the surrounding fluid, and L is the characteristic length of the robot. In order to replicate

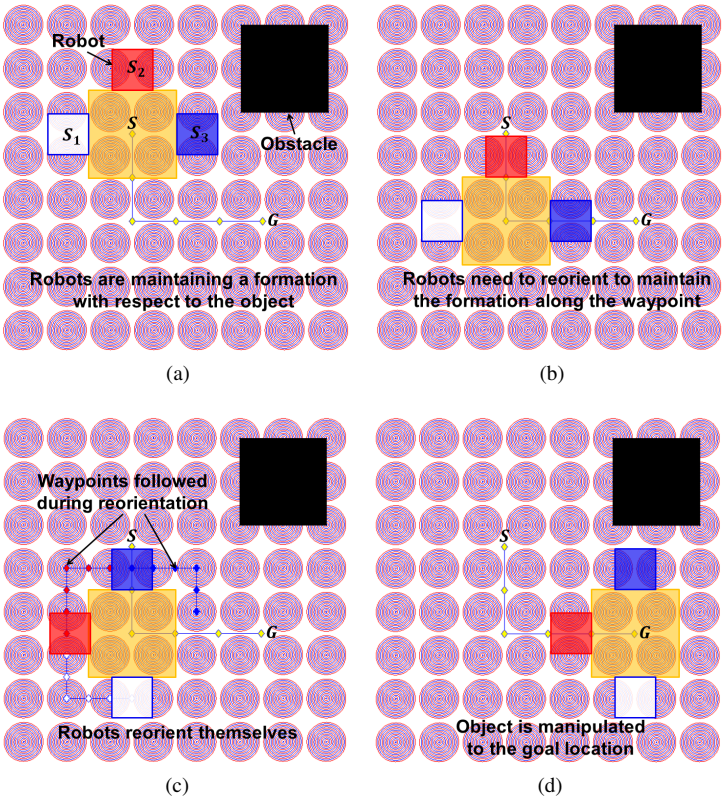

Figure 9: Coordinated manipulation of an object with a team of three robots: (a) Three robots create a formation with the object; (b) The object needs to change the direction of motion to reach to the next waypoint; (c) The robots reorient themselves to maintain the formation; (d) The object is manipulated to the goal location G.

Table 2: Optimization Parameters

Coils	F_x (μN)	F_y (μN)	I_1 (A)	I_2 (A)	I_3 (A)	I_4 (A)
4-Coil System	0.9	0	0.80	0	-0.80	0
64-Coil System	0.7	0	0.12	0.12	-0.12	-0.12

the real world scenario we have introduced Gaussian noise into the measured states of the robot to test the effectiveness of the controller.

In the first experiment, one robot autonomously navigated to a goal location actuated by the global magnetic field generated by the 4-coil system (Fig. 7). The initial location is defined by S and marked with a green "×" (Fig. 7a). Similarly, the respective goal location is defined by G and marked with a yellow "×". The workspace is discritized for the planner. Each grid location is considered as a state that the robot can achieve with the execution of an action. The action set consists of 8 linear actions that can take the robot to a neighboring grid location. The planner computes a collision free path consisting of multiple waypoints w_p marked in white "◊". The PI controller described in section 4.1 tracks the waypoints. Due to the presence of noise, the robot can drift from the waypoint. However, the tuned parameters of the controller are able to track the waypoint by measuring the error and taking corrective measures. The path followed by the controller is shown in Figure 7b.

In the second experiment, three robots are navigated autonomously on a workspace consisting of obstacles. To move multiple robots independently, an array of microcoils have been modeled (Fig. 8). Circular coils are modeled with the same effective length of rectangular coils shown in Figure 5 to utilize the mathematical expressions in literature for computing the resultant magnetic fields. The coils are designed as rectangular shapes for the ease of fabrication. During the computation of the collision-free paths for a robot, the surrounding robots as well as the static objects are considered as obstacles. Since the surrounding robots (obstacles) are always in movement, the environment for the planning is dynamic in nature. Hence, the planner utilizes the re-planning advantage of the D* Lite algorithm (Section 3) to compute the path efficiently. We have considered four actions (top, bottom, right, and left) that can take the robot to a neighboring grid in a discretized workspace. The four actions are used to prevent the robots from navigating through the coils. The adjacent four magnetic coils are taken into consideration during the optimization step to compute the required currents since they have the maximum influence on the robot. The magnetic field created by the distant magnetic coils are negligible and hence are turned off for the particular action. The initial and goal locations are marked as S_i and G_i respectively where $i = 1,2,3$ (Fig. 8a). The collision free waypoints are marked by ◊. The respective controller for each robot tries to track the waypoint at the controller frequency which suffers from a measurement noise. The paths followed by the controller are shown in Figure 8b.

Figure 9 shows the coordianated manipulation of a nonmagnetic object with a team of three robots. The robots create a formation by maintaining a constant orientation with respect to the object during manipulation. The initial formation can be determined based on the size of the object and realized by automatically moving the robots to the respective locations. The collision free path for the object is computed by taking the size of the formation into account. The motions of the robots are restricted to maintain a constant formation. Hence, the individual path for each robot is derived from the computed path for the object. The initial position of the object is marked as S and the robot positions are marked by S_i where $i = 1,2,3$ (Fig. 9a). The robots

need to reorient themselves with respect to the object to change the direction of motion (Fig. 9b) while maintaining the constant formation. The individual paths for the robots are recomputed for reorientation (Fig. 9c). The object is finally manipulated to the goal location at G (Fig. 9d).

Table 2 shows the simulation results in one control loop for both the systems. For the 4-coil system, the robot is located at the waypoint $w_{p,1}$ and has to be navigated to the next waypoint $w_{p,2}$ (Fig. 8b). Both the waypoints are located along the axis of two coils. The two coils along the axis of the motion are switched on while the other two are switched off. One coil applies repulsion force (I_1 = 0.80 A) while the other applies an attraction force (I_3 = -0.80 A) to navigate the robot. The 64-coil system can generate more force with small amount of current since the robot is located much closer to the coil compared to the big coils. Moreover, the robot volume is higher in the later case. For the 64-coil system, the waypoints $w_{p,1}$ and $w_{p,2}$ are located horizontally and the robot is at $w_{p,1}$ (Fig. 8b). Each waypoint is in the middle of four adjacent coils. The two coils on the left of the robot apply a repulsion force ($I_1 = I_2$ = 0.12 A) whereas the coils towards right apply an attraction force ($I_3 = I_4$ = -0.12 A) to navigate the robot from $w_{p,1}$ to $w_{p,2}$(Fig. 8b).

8 CONCLUSIONS AND FUTURE WORKS

With the advent of miniaturization of high-tech products, there is a necessity for high throughput system to assemble micro and nano-scale components. Moreover, the ability to manipulate objects in high volume autonomously can revolutionize the biological experiments. Magnetic fields created by electromagnetic coils are capable of generating a wide range of forces suitable for manipulating objects in microscale. However, generating local magnetic fields and the automated actuation of multiple robots to manipulate a large number of objects independently is challenging.

In this paper, we have developed an approach for autonomous navigation of single and multiple robots in a dynamic environment. The approach starts with planning for collision free waypoints, followed by a controller to compute the required force to actuate the robots towards the waypoints, and an optimization routine to compute the required currents in the electromagnetic coils that can drive the robots. We have also presented the design of a device comprised of an array of 64 microcoils that can generate local magnetic fields for independent actuation of multiple robots. We have conducted extensive simulation experiments to demonstrate the effectiveness of the approach. The parameters used in the simulation are based on extensive previous experimental characterization of the system [29].

In future, we will implement the control of orientation along with the position of the robot to navigate the robot in narrow passages in between obstacles. We will also implement the approach on a physical microcoil array to control multiple microrobots independently towards our ultimate goal to realize a micro-assembly manufacturing station.

ACKNOWLEDGMENT

The authors would like to acknowledge the support of NSF grants IIS-1358446 and IIS-1302283 for this work. Opinions expressed are those of the authors and do not necessarily reflect opinions of the sponsors.

REFERENCES

[1] Chowdhury, S., Švec, P., Wang, C., Seale, K. T., Wikswo, J. P., Losert, W., and Gupta, S. K., 2013. "Automated cell transport in optical tweezers-assisted microfluidic chambers". *IEEE Transactions on Automation Science and Engineering,* ***10***(4), pp. 980–989.

[2] Donald, B. R., Levey, C. G., McGray, C. D., Paprotny, I., and Rus, D., 2006. "An untethered, electrostatic, globally controllable mems micro-robot". *Journal of Microelectromechanical Systems,* ***15***(1), pp. 1–15.

[3] Jing, W., Chen, X., Lyttle, S., Fu, Z., Shi, Y., and Cappelleri, D., 2010. "Design of a magnatostrictive thin microrobot". In Proceedings of ASME International Design Engineering Technical Conferences & Computers and Information in Engineering Conference.

[4] Jing, W., Chen, X., Lyttle, S., Fu, Z., Shi, Y., and Cappelleri, D., 2011. "A magnetic thin film microrobot with two operating modes". In 2011 IEEE International Conference on Robotics and Automation (ICRA), pp. 96–101.

[5] Li, G., Xi, N., Chen, H., Saeed, A., and Yu, M., 2004. "Assembly of nanostructure using afm based nanomanipulation system". In 2004 IEEE International Conference on Robotics and Automation (ICRA'04), pp. 428–433.

[6] Bista, S., Chowdhury, S., Gupta, S. K., and Varshney, A., 2013. "Using GPUs for realtime prediction of optical forces on microsphere ensembles". *Journal of Computing and Information Science in Engineering,* ***13***(3), Apr, p. 031002.

[7] Chowdhury, S., Thakur, A., Švec, P., Wang, C., Losert, W., and Gupta, S., 2014. "Automated manipulation of biological cells using gripper formations controlled by optical tweezers". *IEEE Transactions on Automation Science and Engineering,* ***11***(2), April, pp. 338–347.

[8] Thakur, A., Chowdhury, S., Švec, P., Wang, C., Losert, W., and Gupta, S. K., 2014. "Indirect pushing based automated micromanipulation of biological cells using optical tweezers". *The International Journal of Robotics Research*.

[9] Das, A. N., Zhang, P., Lee, W. H., Popa, D., and Stephanou, H., 2007. "μ^3: multiscale, deterministic micro-nano assembly system for construction of on-wafer microrobots". In 2007 IEEE International Conference on Robotics and Automation, pp. 461–466.

[10] Cappelleri, D., Fu, Z., and Fatovic, M., 2012. "Caging for 2d and 3d micromanipulation". *Journal of Micro-Nano Mechatronics,* ***7***(4), pp. 115–129.

[11] Cappelleri, D. J., and Fu, Z., 2013. "Towards flexible, automated microassembly with caging micromanipulation". In 2013 IEEE International Conference on Robotics and Automation (ICRA), pp. 1427–1432.

[12] Hoover, A. M., and Fearing, R. S., 2007. "Rapidly prototyped orthotweezers for automated microassembly". In 2007 IEEE International Conference on Robotics and Automation,, pp. 812–819.

[13] Probst, M., Hürzeler, C., Borer, R., and Nelson, B. J., 2009. "A microassembly system for the flexible assembly of hybrid robotic mems devices". *International Journal of Optomechatronics,* ***3***(2), pp. 69–90.

[14] Fatikow, S., Seyfried, J., Buerkle, A., Schmoeckel, F., et al., 2000. "A flexible microrobot-based microassembly station". *Journal of Intelligent and Robotic Systems,* ***27***(1-2), pp. 135–169.

[15] Bohringer, K.-F., Goldberg, K., Cohn, M., Howe, R., and Pisano, A., 1998. "Parallel microassembly with electrostatic force fields". In 1998 IEEE International Conference on Robotics and Automation, pp. 1204–1211.

[16] Diller, E., Pawashe, C., Floyd, S., and Sitti, M., 2011. "Assembly and disassembly of magnetic mobile micro-robots towards deterministic 2-d reconfigurable micro-systems". *The International Journal of Robotics Research.*

[17] Diller, E., Floyd, S., Pawashe, C., and Sitti, M., 2012. "Control of multiple heterogeneous magnetic microrobots in two dimensions on nonspecialized surfaces". *IEEE Transactions on Robotics,* ***28***(1), pp. 172–182.

[18] Pelrine, R., Wong-Foy, A., McCoy, B., Holeman, D., Mahoney, R., Myers, G., Herson, J., and Low, T., 2012. "Diamagnetically levitated robots: An approach to massively parallel robotic systems with unusual motion properties". In 2012 IEEE International Conference on Robotics and Automation (ICRA),, pp. 739–744.

[19] Peng, T., Balijepalli, A., Gupta, S. K., and LeBrun, T., 2007. "Algorithms for on-line monitoring of micro spheres in an optical tweezers-based assembly cell". *Journal of Computing and Information Science in Engineering,* ***7***(4), pp. 330–338.

[20] Banerjee, A. G., Pomerance, A., Losert, W., and Gupta, S. K., 2010. "Developing a Stochastic Dynamic Programming Framework for Optical Tweezer-Based Automated Particle Transport Operations". *IEEE Transactions on Automation Science and Engineering,* ***7***(2), Apr, pp. 218–227.

[21] Banerjee, A. G., Chowdhury, S., Losert, W., and Gupta, S. K., 2012. "Real-time path planning for coordinated transport of multiple particles using optical tweezers". *IEEE Transactions on Automation Science and Engineering,* ***9***(4), Oct, pp. 669 –678.

[22] Banerjee, A., Chowdhury, S., and Gupta, S., 2014. "Optical tweezers: Autonomous robots for the manipulation of biological cells". *IEEE Robotics Automation Magazine,* ***21***(3), Sept, pp. 81–88.

[23] Hu, W., Ishii, K. S., and Ohta, A. T., 2011. "Micro-assembly using optically controlled bubble microrobots". *Applied Physics Letters,* ***99***(9), pp. –.

[24] Sariola, V., Jaaskelainen, M., and Zhou, Q., 2010. "Hybrid microassembly combining robotics and water droplet self-alignment". *IEEE Transactions on Robotics,* ***26***(6), pp. 965–977.

[25] Jing, W., Pagano, N., and Cappelleri, D. J., 2012. "A micro-scale magnetic tumbling microrobot". In ASME 2012 International Design Engineering Technical Conferences and Computers and Information in Engineering Conference, American Society of Mechanical Engineers, pp. 187–196.

[26] Jing, W., Pagano, N., and Cappelleri, D. J., 2013. "A tumbling magnetic microrobot with flexible operating modes". In 2013 IEEE International Conference on Robotics and Automation (ICRA), pp. 5514–5519.

[27] Jing, W., Pagano, N., and Cappelleri, D. J., 2013. "A novel micro-scale magnetic tumbling microrobot". *Journal of Micro-Bio Robotics,* ***8***(1), pp. 1–12.

[28] Steager, E. B., Sakar, M. S., Magee, C., Kennedy, M., Cowley, A., and Kumar, V., 2013. "Automated biomanipulation of single cells using magnetic microrobots". *The International Journal of Robotics Research,* ***32***(3), pp. 346–359.

[29] Jing, W., and Cappelleri, D. J., 2014. "Towards functional mobile magnetic microrobots". In *Small-Scale Robotics. From Nano-to-Millimeter-Sized Robotic Systems and Applications*. Springer, pp. 81–100.

[30] Jing, W., and Cappelleri, D., 2014. "Incorporating in-situ force sensing capabilities in a magnetic microrobot". In 2014 IEEE/RSJ International Conference on Intelligent Robots and Systems (IROS 2014),, pp. 4704–4709.

[31] LaValle, S. M., 2006. *Planning algorithms*. Cambridge university press.

[32] Hart, P., Nilsson, N., and Raphael, B., 1968. "A formal basis for the heuristic determination of minimum cost paths". *IEEE Trans. Syst. Sci Cybern.,* ***4***(2), Jul, pp. 100 –107.

[33] LaValle, S. M., and Kuffner Jr, J. J., 2000. "Rapidly-exploring random trees: Progress and prospects".

[34] Koenig, S., and Likhachev, M., 2002. "D* lite". In AAAI Conference of Artificial Intelligence, pp. 476–483.

[35] Cappelleri, D. J., Efthymiou, D., Goswami, A., Vitoroulis, N., and Zavlanos, M., 2014. "Towards mobile microrobot swarms for additive micromanufacturing". *International Journal of Advanced Robotic Systems,* ***11***, p. 150.

[36] Jing, W., and Cappelleri, D., 2014. "A magnetic microrobot with in situ force sensing capabilities". *Robotics,* ***3***(2), pp. 106–119.